Differential cross sections for neutrino scattering on ^{12}C

E. Kolbe
Departement für Physik und Astronomie der Universität Basel, Switzerland
(Received 4 June 1996)

Differential cross sections for neutrino scattering on ^{12}C are calculated within the (continuum) random phase approximation model. The charged current (ν_e, e^-) and (ν_μ, μ^-) capture reactions on ^{12}C are measured by the LSND Collaboration at LAMPF. We investigate and discuss the merits of such studies, especially the information that can be extracted from data for differential neutrino scattering cross sections. [S0556-2813(96)04910-2]

PACS number(s): 25.30.Pt, 13.15.+g, 14.60.Pq, 23.40.Bw

I. INTRODUCTION

Although first attempts were started in the early 1970s, it took until the year 1990 that measurements of neutrino-nucleus scattering cross sections (with an error $\leqslant 20\%$) became feasible. By that time an experimental group (E225) at LAMPF [1] determined both the inclusive $^{12}\mathrm{C}(\nu_e, e^-)X$ cross section and the exclusive contribution to the ^{12}N ground state. Soon afterwards also the KARMEN Collaboration [2,3] measured these cross sections, and, on top of that, observed a neutral current excitation of a nucleus, the $^{12}\mathrm{C}(\nu, \nu')\,^{12}\mathrm{C}^*(1^+,1;15.11\ \mathrm{MeV})$ reaction. Since 1993 the LSND Collaboration at LAMPF [4] is using, in addition to the low energy neutrinos ($E_\nu \leqslant 52.8$ MeV) stemming from pion decay at rest, neutrinos with higher energies ($E_\nu \leqslant 300$ MeV) from pion-in-flight decay to study neutrino induced reactions on ^{12}C. Within the last four years both groups significantly improved their setup and collected more data for better statistics.

Already in the 1990 experiment Allen *et al.* [1] took data for the angular distribution of the $^{12}\mathrm{C}(\nu_e, e^-)^{12}\mathrm{N}_{\mathrm{g.s.}}$ cross section (see, e.g., Fig. 2 in Ref. [1]). And as the liquid scintillator neutrino detector is, like the E225 experiment, capable of determining the direction of the outgoing electron via observing its Čerenkov light cone, we expect further and improved data to come up soon.

For simplicity of notation let us define that the term ''differential cross section'' will be used in the following to denote the scattering angle dependent cross section $(d\sigma/d\Omega)$ as well as the cross section differential for the energy of the outgoing lepton $(d\sigma/d\epsilon_f)$ or both $(d^2\sigma/d\Omega d\epsilon_f)$.

The purpose of this paper is to investigate what we can learn from measuring differential (ν_l, l^-) cross sections $(l = e, \mu)$ on ^{12}C, including the question whether or how they are linked to the detection of neutrino oscillations and to solving the discrepancy between theory and experiment concerning the $^{12}\mathrm{C}(\nu_\mu, \mu^-)X$ reaction [5–7].

The paper is organized as follows. The theoretical basis of our calculations has been presented in detail in previous papers [8,9]. In Sec. II we therefore just summarize the basic features of continuum random phase approximation (RPA) and state the key formulas. In the first part of Sec. III angular distributions for neutrino induced reactions are generally treated. This is the prerequisite to a second part, where we discuss which information could be extracted from such measurements. Section IV describes electron energy spectra and angular distributions for $^{12}\mathrm{C}(\nu_e, e^-)X$ reactions. Here we focus on the difference between the expected standard events and events stemming from $\nu_\mu \rightarrow \nu_e$ oscillations. Finally Sec. V is given over to a summary.

II. BASIC INGREDIENTS

Due to the smallness of the Fermi coupling constant, neutrino scattering cross sections (and other weak observables like muon capture rates) can be accurately calculated within first-order Born approximation by application of the Feynman rules and a multipole expansion of the transition operators as outlined in Ref. [10]. For the low neutrino energies and small momenta ($|\vec{q}| \leqslant 400$ MeV/c) transferred in the reactions calculated here, the weak Hamiltonian can be written, according to the standard model, in the usual (effective) current-current form. The second basic ingredient is the initial and final nuclear states, which we describe within the continuum random phase approximation (RPA). As the model has been dealt with in detail in Refs. [8,9], it is appropriate that we just briefly outline its features in the following. In this approach the usual RPA treatment is combined with a correct description of the particle states in the continuum, i.e., the excited many-body states are coherent superpositions of one-particle–one-hole (1p-1h) excitations obeying the proper Coulomb boundary conditions for scattering states. Its basic properties can be summarized by (1) the nuclear ground state is well described, (2) the excited states are generic continuum states of 1p-1h structure, (3) final state interactions are accounted for with a realistic (finite range) residual interaction derived from the Bonn meson exchange potential [11,12], (4) this model has been shown [13,9] to yield a good description of the giant (dipole and spin-dipole) resonances in light nuclei, e.g., in ^{12}C and ^{16}O, which are expected to dominate the low energy neutrino scattering cross sections, (5) continuum RPA has been found to reproduce well the total muon capture rates in nuclei like ^{12}C, ^{16}O, and ^{40}Ca [14].

As we will refer to it in the following section, we write down the neutrino scattering cross section formula as derived in [10],

$$\left(\frac{d^{[2]}\sigma_{i\to f}}{d\Omega[d\omega]}\right)_{\nu/\bar{\nu}} = \frac{G^2}{\pi}\,\frac{|\vec{k}_f|\epsilon_f}{2J_i+1}F(Z,\epsilon_f) \times\left\{\sum_{J=0}^{\infty}\eta_{CL}^J+\sum_{J=1}^{\infty}\eta_{TI}^J\right\}, \tag{1}$$

$$\eta_{CL}^J := (1+a\cos\Theta)|\langle J_f\|\hat{\mathcal{M}}_J(q)\|J_i\rangle|^2+(1+a\cos\Theta -2b\sin^2\Theta)|\langle J_f\|\hat{\mathcal{L}}_J(q)\|J_i\rangle|^2+\left[\frac{\omega}{q}(1+a\cos\Theta)+c\right] \times 2\mathrm{Re}\langle J_f\|\hat{\mathcal{L}}_J(q)\|J_i\rangle\langle J_f\|\hat{\mathcal{M}}_J(q)\|J_i\rangle^*, \tag{2}$$

$$\eta_{TI}^J := (1-a\cos\Theta+b\sin^2\Theta)[|\langle J_f\|\hat{\mathcal{T}}_J^{\mathrm{mag}}(q)\|J_i\rangle|^2 +|\langle J_f\|\hat{\mathcal{T}}_J^{\mathrm{el}}(q)\|J_i\rangle|^2]\mp\left[\frac{\epsilon_i+\epsilon_f}{q}(1-a\cos\Theta)-c\right] \times 2\mathrm{Re}\langle J_f\|\hat{\mathcal{T}}_J^{\mathrm{mag}}(q)\|J_i\rangle\langle J_f\|\hat{\mathcal{T}}_J^{\mathrm{el}}(q)\|J_i\rangle^*, \tag{3}$$

where we have used the abbreviations

$$a := \frac{|\vec{k}_f|}{\epsilon_f} = \sqrt{1-\left(\frac{m_f c^2}{\epsilon_f}\right)^2},$$

$$b := \frac{\epsilon_i\epsilon_f a^2}{q^2},$$

$$c := \frac{(m_f c^2)^2}{q\epsilon_f},$$

$$\epsilon_f := \epsilon_i-\omega, \tag{4}$$

and the absolute value of the (three-) momentum transfer is given by

$$q := |\vec{q}| = \sqrt{\omega^2+2\epsilon_i\epsilon_f(1-a\cos\Theta)-(m_f c^2)^2}. \tag{5}$$

Here $\Theta,\omega,\epsilon_i,\epsilon_f,\vec{k}_f,m_f$ denote scattering angle, excitation energy of the nucleus, energy of the incoming neutrino and energy, momentum and mass of the outgoing lepton, respectively. The charge ($\hat{\mathcal{M}}_J$), longitudinal ($\hat{\mathcal{L}}_J$), and transverse operators ($\hat{\mathcal{T}}_J^{\mathrm{el}}$,$\hat{\mathcal{T}}_J^{\mathrm{mag}}$) in the reduced matrix elements stem from the multipole expansion of the weak hadronic current (see Ref. [10]). The Fermi function $F(Z,\epsilon_f)$ takes account of the Coulomb final state interaction between nucleus and final lepton in the case of charged current reactions. Note that the interference term between vector and axial vector current in the lower line of Eq. (3) has a negative (positive) sign for (anti)neutrino scattering due to their different helicities. The square brackets on the left-hand side of Eq. (1) indicate that the cross section is a double differential ($d\Omega d\omega$) for excitation of states lying in the continuum.

If the mass of the outgoing lepton can be neglected, i.e., in the extreme relativistic limit [ERL, this applies for (ν_e,e^-) reactions], the cross section formula reduces to the simpler form:

$$\left(\frac{d^{[2]}\sigma_{i\to f}}{d\Omega[d\omega]}\right)_{\nu/\bar{\nu}} = \frac{2G^2\epsilon_f^2}{\pi}\,\frac{1}{2J_i+1}F(Z,\epsilon_f) \times\left\{\sum_{J=0}^{\infty}\eta_{CL}^J+\sum_{J=1}^{\infty}\eta_{TI}^J\right\}, \tag{6}$$

$$\eta_{CL}^J := \cos^2\frac{\Theta}{2}\left|\left\langle J_f\middle\|\hat{\mathcal{M}}_J(q)+\frac{\omega}{q}\hat{\mathcal{L}}_J(q)\middle\|J_i\right\rangle\right|^2, \tag{7}$$

$$\eta_{TI}^J := \left(-\frac{q_\mu^2}{2q^2}\cos^2\frac{\Theta}{2}+\sin^2\frac{\Theta}{2}\right)[|\langle J_f\|\hat{\mathcal{T}}_J^{\mathrm{mag}}(q)\|J_i\rangle|^2 +|\langle J_f\|\hat{\mathcal{T}}_J^{\mathrm{el}}(q)\|J_i\rangle|^2] \mp\sin\frac{\Theta}{2}\sqrt{\frac{-q_\mu^2}{q^2}\cos^2\frac{\Theta}{2}+\sin^2\frac{\Theta}{2}} \times 2\mathrm{Re}\langle J_f\|\hat{\mathcal{T}}_J^{\mathrm{mag}}(q)\|J_i\rangle\langle J_f\|\hat{\mathcal{T}}_J^{\mathrm{el}}(q)\|J_i\rangle^*, \tag{8}$$

with momentum transfer

$$q := |\vec{q}| = \sqrt{\omega^2+4\epsilon_i\epsilon_f\sin^2\frac{\Theta}{2}}. \tag{9}$$

The following features of the cross section formulas are important

(1) Due to the current-current form of the weak Hamiltonian the contributions to the cross section are products of leptonic (i.e., kinematical terms, as the leptons are pointlike) and hadronic matrix elements.

(2) Equations (6)–(8) can be compared with the cross section formula for electron scattering (see, e.g., Ref. [15]). In close analogy to the longitudinal and transverse response functions $R_L(q,\omega)$ and $R_T(q,\omega)$ specified there, one is led to define the weak response functions for neutrino scattering by

$$R_{CL}(q,\omega) := \left|\left\langle J_f\middle\|\hat{\mathcal{M}}_J(q)+\frac{\omega}{q}\hat{\mathcal{L}}_J(q)\middle\|J_i\right\rangle\right|^2, \tag{10}$$

$$R_T(q,\omega) := |\langle J_f\|\hat{\mathcal{T}}_J^{\mathrm{mag}}(q)\|J_i\rangle|^2+|\langle J_f\|\hat{\mathcal{T}}_J^{\mathrm{el}}(q)\|J_i\rangle|^2, \tag{11}$$

$$R_I(q,\omega) := 2\mathrm{Re}\langle J_f\|\hat{\mathcal{T}}_J^{\mathrm{mag}}(q)\|J_i\rangle\langle J_f\|\hat{\mathcal{T}}_J^{\mathrm{el}}(q)\|J_i\rangle^*. \tag{12}$$

Furthermore, in the general case where the mass of the outgoing lepton cannot be neglected, the response $R_{CL}(q,\omega)$ in Eq. (10) must be split up in three functions $R_C(q,\omega)$, $R_L(q,\omega)$, and $R_{CLI}(q,\omega)$ corresponding to the three hadronic matrix elements given in Eq. (2), respectively. Note that, in principle, also $R_{CL}(q,\omega)$ in Eq. (10) must be split up in this way, because, due to the leptonic factor ω/q in front of the operator $\hat{\mathcal{L}}_J$, this nuclear response function is not purely hadronic. For the sake of simplicity we have chosen the definition in Eq. (10), though.

(3) In the ERL described by Eqs. (6)–(8) only the transverse operators contribute to the backward scattering $\Theta\to 180°$ cross section, while for forward scattering $\Theta\to 0°$ there are only Coulomb and longitudinal contributions to the cross section. This reflects the fact that the spin transfer to the nucleus along the momentum transfer $\vec{q}$ from

an incoming left-handed neutrino is zero (i.e., longitudinal) for an outgoing extreme relativistic (and therefore also left-handed) lepton in the forward direction. And it must be one (i.e., transverse), if the lepton goes in the opposite (backward) direction.

Finally, to compare with the data, the differential cross sections in Eqs. (1) and (6) must be folded with the normalized energy distribution $n_i(\epsilon_i)$ of the incoming neutrinos:

$$\frac{d^{[2]}\overline{\sigma}}{d\Omega[d\omega]}([\omega,]\Theta)=\int_0^\infty \frac{d^{[2]}\sigma}{d\Omega[d\omega]}([\omega,]\Theta,\epsilon_i)n_i(\epsilon_i)d\epsilon_i\,, \tag{13}$$

and, for excitation of states lying in the continuum, one has to integrate over the excitation energy ω:

$$\frac{d\overline{\sigma}}{d\Omega}(\Theta)=\int_{\omega_{\rm thres}}^\infty \frac{d^2\overline{\sigma}}{d\Omega d\omega}(\omega,\Theta)d\omega. \tag{14}$$

III. RESULTS

We start with a (more academic) description and discussion of differential cross sections for neutrino induced reactions on nuclei, ignoring for the moment whether they can be measured or not. Note that in most of the following plots the differential cross sections were normalized by the corresponding total cross sections in order to compare all results on a linear scale. For completeness and to be aware of the order of magnitude, we recollect the total cross sections calculated within continuum RPA, although already published [16,5], in Table I. Here we also list other theoretical results and compare with the latest data (available to the author). The agreement between continuum RPA theory and experiment is generally very nice, except the discrepancy by a factor of 1.7 for the ^{12}C$(\nu_\mu,\mu^-)X$ reaction.

Figure 1 shows the calculated differential cross sections for charged-current excitations of ^{12}C as a function of the scattering angle. In the upper diagram [Fig. 1(a)] the exclusive reactions to the ^{12}N ground state (solid lines) are plotted. While the (ν_e,e^-) cross section (thick line) is slightly backward peaked, we find that the (ν_μ,μ^-) cross section (thin line) is strongly forward peaked. This arises from the weight of the Coulomb-plus-longitudinal (in the following denoted by σ_{CL}) and transverse (σ_{TI}) contributions, which are shown as dashed and dotted curves in Fig. 1, too. They correspond to the first and second sum in Eq. (1), respectively. Note that, while the transverse contribution to the (ν_e,e^-) cross section according to the kinematical factor in Eq. (8) vanishes at scattering angle $\Theta=0°$, this does not happen for the (ν_μ,μ^-) reaction, due to the non-negligible mass of the muon.

TABLE I. Comparison of measured and calculated total cross sections for neutrino capture reactions on ^{12}C in units of 10^{-42} cm^2. The results of this work are labeled by an asterisk.

Reaction	Theory	Ref.	Expt.	Ref.
^{12}C$(\nu_\mu,\mu^-)X$	1925	[*]	1130 ± 30(stat)±180(syst)	[18]
	1900	[6]		
	1310	[17]		
^{12}C$(\nu_\mu,\mu^-)^{12}$N$_{\rm g.s.}$	63	[*]	64 ± 10(stat)±10(syst)	[18]
^{12}C$(\nu_e,e^-)^{12}$N*	3.7	[19]	6.1 ± 0.9(stat)±1.1(syst)	[20]
	6.3	[*]	6.0 ± 0.6(stat)±0.8(syst)	[18]
	9.8	[21]		
^{12}C$(\nu_e,e^-)^{12}$N$_{\rm g.s.}$	9.4	[19]	10.5 ± 1.0(stat)±1.0(syst)	[1]
	9.2	[22]	9.1 ± 0.5(stat)±0.8(syst)	[20]
	9.3	[*]	9.1 ± 0.4(stat)±0.9(syst)	[18]
	8.0	[23]		

Unfortunately the ^{12}C$(\nu_e,e^-)^{12}$N$_{\rm g.s.}$ cross section [thick line in Fig. 1(a)] cannot quantitatively be compared with the data in Fig. 2(b) of Ref. [1], because, due to its layered structure, the E225 detector had a very limited resolution for electrons produced around $\Theta=90°$. However, it can be read off the solid line in Fig. 1(a) that the calculated ratio of backward to forward cross section is slightly smaller than 2:1, which is in good agreement with the data.

Our calculation can also be compared with the new preliminary LSND data [18] for the angular distribution, which do not exhibit the unfavorable limited resolution around $\Theta=90°$. However, the error bars are still too big to allow a cogent test of the theory. Qualitatively, drawing a straight line through the data, one can estimate a value of 1.7 ± 0.2 for the ratio of backward to forward scattering. This is in agreement with the calculated result.

The lower diagram [Fig. 1(b)] shows the reactions plotted in Fig. 1(a), but now for the excited states in ^{12}N (denoted by

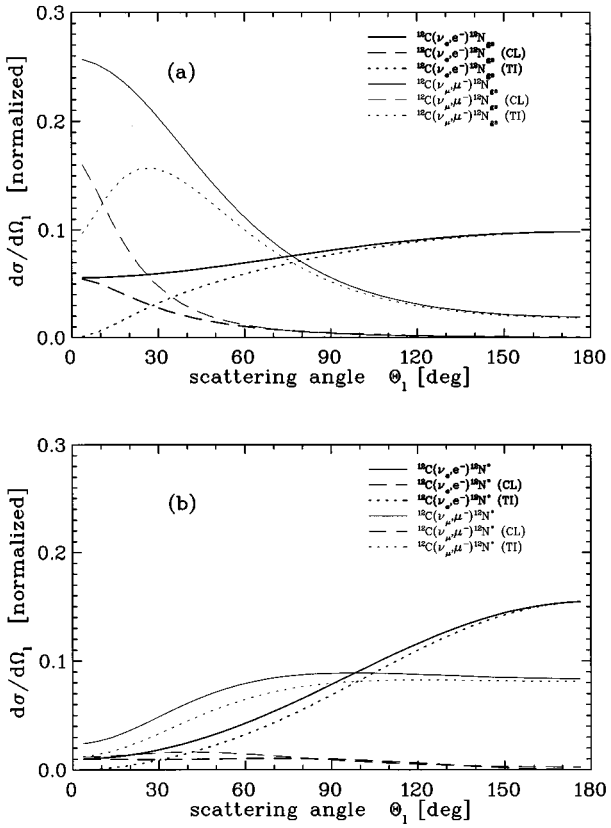

FIG. 1. Normalized differential cross sections as a function of the neutrino-lepton scattering angle. In the upper diagram (a) the angular distributions for the exclusive reactions to the ^{12}N ground state are plotted, the lower diagram (b) shows the same for ^{12}C$(\nu_l,l^-)^{12}$N* reactions.

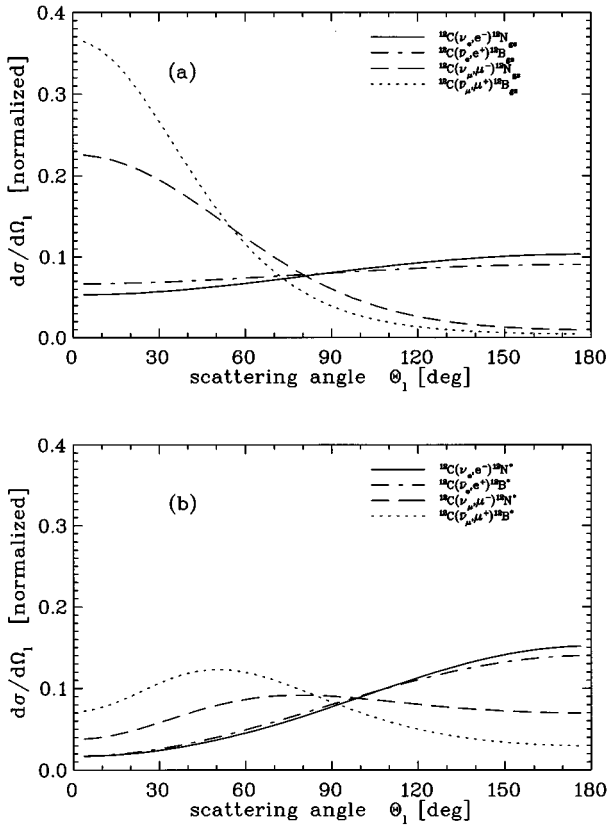

FIG. 2. Comparison of differential cross sections for neutrino and antineutrino scattering. The upper diagram (a) shows the angular distributions for the exclusive reactions [^{12}C(ν_l,l^-)^{12}N$_{g.s.}$ vs ^{12}C($\overline{\nu_l}$,l^+)^{12}B$_{g.s.}$], in the lower diagram (b) $d\sigma/d\Omega_l$ is plotted for ^{12}C(ν_l,l^-)^{12}N* and ^{12}C($\overline{\nu_l}$,l^+)^{12}B* reactions.

^{12}N*), i.e., these are the *inclusive minus ground state* cross sections. For both (ν_μ,μ^-) and (ν_e,e^-) reactions the dominant contributions come from the transverse response. Note that the strong backward peaking of the ^{12}C(ν_e,e^-)^{12}N* cross section, which at first glance might be surprising, can be attributed to the fundamental conserved vector current (CVC) hypothesis, as has been pointed out by Donnelly [19]. The argument is based on Adler's theorem [24], which states that in the extreme relativistic limit the forward (anti)neutrino cross section only depends on the divergences of the vector and axial vector hadronic currents. If the vector current is conserved, only the divergence of the axial vector term contributes to the forward scattering cross section. Furthermore the Coulomb and longitudinal-multipole operators for the axial current are only involved in transitions to ^{12}N* states of unnatural parity, because they have parity $(-)^{J+1}$ [10] and act on the initial $J_i^\pi = 0^+$ ^{12}C ground state. By a multipole analysis of the ^{12}C(ν_e,e^-)^{12}N* reaction we find that dominantly 1^- (48% of the strength) and 2^- (44%) states in ^{12}N* are excited. Hence, if CVC is fulfilled, the forward scattering cross section measures only the σ_{CL} contribution from the excitation of 2^- states and therefore should be small.

In Fig. 2 we compare neutrino and antineutrino capture reactions on ^{12}C. As the interference term in the lower line of Eq. (3) turns out to have a negative sign for the plotted reactions, we find that the antineutrino cross sections are smaller (destructive interference) than the neutrino cross sections, where vector and axial vector current interfere constructively. Combined with the backward peaking of the kinematical (or leptonic) factor in Eq. (3) this causes the differential cross sections for antineutrinos to be more forward peaked (or less backward peaked) than for neutrinos.

TABLE II. Average value of the momentum transfer to the nucleus for neutrino capture reactions and muon capture on ^{12}C. The abbreviations DAR and DIF stand for decay at rest and decay in flight.

Reaction	ν source	$\langle\lvert\vec{q}\rvert\rangle$ (MeV/c)
^{12}C(ν_e,e^-)^{12}N$_{g.s.}$	DAR	47.3
^{12}C(ν_e,e^-)^{12}N*	DAR	53.6
^{12}C(ν_μ,μ^-)^{12}N$_{g.s.}$	DIF	131.0
^{12}C(ν_μ,μ^-)^{12}N*	DIF	206.8
^{12}C(μ^-,ν_μ)^{12}B*	(m_μ)	83.3

Reflecting the product form of Eqs. (1)–(3) and (6)–(8) we generally find for (ν_e,e^-) reactions that the leptonic (kinematical) factors vary more strongly as functions of the scattering angle Θ than their hadronic counterparts, i.e., the nuclear response functions. Therefore, the shapes of the σ_{CL} and σ_{TI} contributions (thick dashed and dotted curves in Fig. 1) are determined by the kinematical factors. Their monotonic decrease (increase) as a function of Θ in the range [0–1] can easily be seen from their analytic expressions in Eqs. (7) and (8). Due to the non-negligible mass, the kinematical terms for (ν_μ,μ^-) vary less strongly [compare analytic expressions in Eqs. (2) and (3) and Eqs. (7) and (8)], and the hadronic response controls the shape of σ_{CL} and σ_{TI}.

According to Eqs. (5) and (9) the momentum transfer is fixed by the scattering angle for given excitation energy ω and neutrino energy ϵ_i. Therefore the momentum transfer distribution of the reaction depends on the shape of the differential cross section (or vice versa). Weighting the transferred momenta with the corresponding differential cross sections we determined their distributions and mean values for the reactions plotted in Fig. 1 and for muon capture. Or, in simple terms, we calculated $d\sigma/dq$ and $d\omega_\mu/dq$, the cross sections and muon capture rate differential for the momentum transfer. From Table II we can gather that the average momentum transfer in (ν_μ,μ^-) reactions is significantly higher than in (ν_e,e^-) reactions, while the average momentum transferred in muon capture lies between these values. Concerning the discrepancy between theory and experiment for the total ^{12}C(ν_μ,μ^-)X reaction cross section, the numbers in Table II deliver the important information at which momentum transfer one should perform further tests of the theoretical models (e.g., by comparison with electron scattering data). Work in this direction is in progress.

The momentum dependences plotted in Fig. 3 also present the *range* of momentum transfer relevant for a reaction. While muon capture (dotted line) analyses the nuclear response functions in a small range between 80 and 90 MeV/c, the dashed curve for the ^{12}C(ν_e,e^-)^{12}N* reaction extends over a wider range centered around $\approx$50 MeV/c. The broad distribution for the ^{12}C(ν_μ,μ^-)^{12}N* reaction cross section (solid line) mirrors the flatness of the corre-

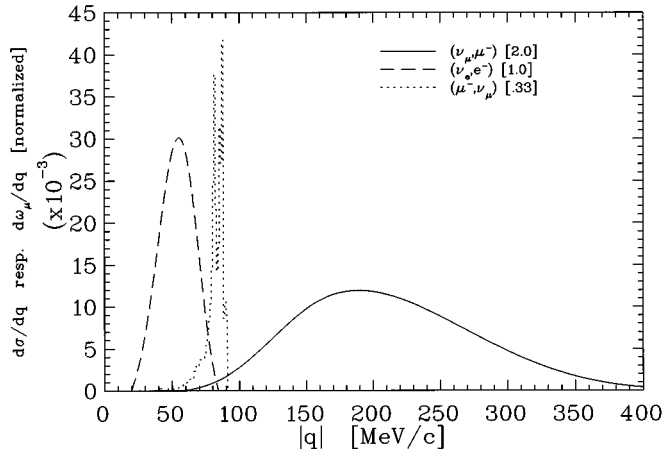

FIG. 3. Momentum transfer dependences for the $^{12}\mathrm{C}(\nu_e,e^-)^{12}\mathrm{N}^*$ and $^{12}\mathrm{C}(\nu_\mu,\mu^-)^{12}\mathrm{N}^*$ reactions ($d\sigma/dq$) and for the $^{12}\mathrm{C}(\mu^-,\nu_\mu)^{12}\mathrm{B}^*$ muon capture rate ($d\omega_\mu/dq$). The curves are normalized by the total cross sections-capture rates and furthermore multiplied by the factors in square brackets.

sponding differential cross section in Fig. 1(b).

To illustrate what can be learned from measurements of angular distributions we present Fig. 4. Here we investigated the effect on the differential cross section caused by a 50% reduction of the σ_{CL} term. This corresponds, e.g., to the situation found in electron scattering, where a theoretical model could yield a wrong result for the ratio of transverse to longitudinal response contributions. The solid and dash-dotted curves show that this would clearly change the shape of the angular distribution for the $^{12}\mathrm{C}(\nu_e,e^-)^{12}\mathrm{N}_{\mathrm{g.s.}}$ reaction. Especially the ratio of backward to forward scattering would rise by a factor of about 2. We find the same factor of 2 for the $^{12}\mathrm{C}(\nu_e,e^-)^{12}\mathrm{N}^*$ reaction (dotted and dashed lines), but the small cross section in the forward direction will hardly be measurable.

This situation leads to the general question whether and how it is possible to separate the weak longitudinal and transverse response in (anti)neutrino scattering. In electron scattering the benefits of such a separation, i.e., the measurement of detailed information on the target dynamics, are well

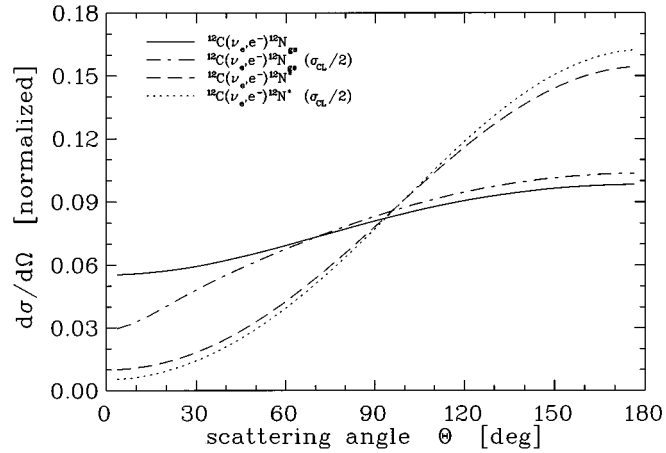

FIG. 4. Effect of a reduction of the Coulomb and longitudinal response on the differential cross sections for the $^{12}\mathrm{C}(\nu_e,e^-)^{12}\mathrm{N}_{\mathrm{g.s.}}$ and $^{12}\mathrm{C}(\nu_e,e^-)^{12}\mathrm{N}^*$ reactions.

known and corresponding experiments have been performed over the last decade [25]. At first glance an analysis analogous to the Rosenbluth-decomposition in electron scattering might suggest itself. But a severe problem comes from the fact that the initial neutrino energy distribution is folded with the response functions and kinematical factors [Eq. (13)]; this does not allow one to extract the responses for a fixed set of ω and q. From a mathematical point of view the folding operation in Eq. (13), which smears the response, cannot be inverted.

However, a solution of this problem can easily be found for the exclusive $^{12}\mathrm{C}(\nu_e,e^-)^{12}\mathrm{N}_{\mathrm{g.s.}}$ reaction. Here the excitation energy of the nucleus ω is constant and a measurement of the double differential cross section $d^2\sigma/d\Omega d\epsilon_f$ will also fix the initial energy of the neutrino by energy conservation. So the $n_i(\epsilon_i)$ spectrum factor is known and the integral in Eq. (13) breaks down. By use of Eq. (9) we obtain for the measured sets $(\epsilon_{f_n},\Theta_n)$ the corresponding momentum transfers q_n or the sets (q_n,Θ_n). Then a binning of q_n into suitable ranges of momentum transfer will allow one to draw for each bin a Rosenbluth plot. In the general case of Eqs. (1)–(3) this would consist of tracing $d^2\sigma/d\Omega d\epsilon_f$ divided by $n_i(\epsilon_i)$ and by the prefactor on the right-hand side in Eq. (1) versus a trigonometric function in Θ (e.g., $\cos\Theta$) to separate the five response functions $R_C(q,\omega)$, $R_L(q,\omega)$, $R_{CLI}(q,\omega)$, $R_T(q,\omega)$, and $R_I(q,\omega)$. However, such a five-parameter fit is very unlikely to be practiced, because, due to the tiny cross sections, we do not expect precise input data from the experiment. Furthermore, it will probably be impossible to measure the outgoing angle for muons, because their energies are too low to produce enough Cerenkov light in the LSND detector. Therefore we confine the discussion in the following to the extreme relativistic limit and consider the three response functions given in Eqs. (10)–(12). Here the Rosenbluth separation can be done by plotting the quantity:

$$\frac{(d^2\sigma_{i\to f}/d\Omega d\epsilon_f)}{(2G^2\epsilon_f^2/\pi)[F(Z,\epsilon_f)/(2J_i+1)]n_i(\omega+\epsilon_f)\cos^2(\Theta/2)} \tag{15}$$

as a function of $\tan^2(\Theta/2)$.

Note that the response function $R_I(q,\omega)$ in Eq. (12) could also be determined by measuring neutrino and antineutrino cross sections, but experiments with neutrino and antineutrino sources of the same type are presently not available. On the other hand it can be seen in Fig. 2 that for (ν_e,e^-) reactions the difference between neutrino and antineutrino scattering is small and therefore the interference term in first order is negligible. Then we are left with the two response functions in Eqs. (10) and (11), which again can be separated by plotting the quantity in Eq. (15) versus $\tan^2(\Theta/2)$. In this case $R_T(q,\omega)$ is the slope and $R_{CL}(q,\omega)-(q_\mu^2/2q^2)R_T(q,\omega)$ the intercept of a linear fit to the data. Finally, following Ref. [25], another method for the separation of $R_{CL}(q,\omega)$ and $R_T(q,\omega)$ is given by plotting the quantity:

$$\frac{(d^2\sigma_{i\to f}/d\Omega d\epsilon_f)\,\eta}{(2G^2\epsilon_f^2/\pi)[F(Z,\epsilon_f)/(2J_i+1)]n_i(\omega+\epsilon_f)\cos^2(\Theta/2)} = \eta R_{CL}(q,\omega)+\left(\frac{-q_\mu^2}{2q^2}\right)R_T(q,\omega) \tag{16}$$

as a function of the argument η defined as

$$\eta := \left[1 + \left(\frac{2q^2}{-q_\mu^2} \right) \tan^2 \frac{\Theta}{2} \right]^{-1} . \tag{17}$$

For decreasing scattering angle Θ from 180° to 0° the variable η rises from 0 to 1 and is correlated to the longitudinal component of the polarization of the exchanged virtual W boson. Then $R_{CL}(q,\omega)$ is the slope and $(-q_\mu^2/2q^2)R_T(q,\omega)$ the intercept of a linear fit to the data.

For the nonexclusive transitions the situation is even worse, here we have an additional folding from the integration in Eq. (14). But, presumed that a measurement of the double differential cross section $d^2\sigma/d\Omega d\epsilon_f$ can be done, theoretical nuclear models can be applied to map the measured sets $(\epsilon_{f_n},\Theta_n)$ onto the corresponding average excitation energy $\overline{\omega_n}$ and average momentum transfer $\overline{q_n}$ or the triplet $(\overline{q_n},\overline{\omega_n},\Theta_n)$. Then a binning of the sets $(\overline{q_n},\overline{\omega_n})$ into suitable ranges of excitation energy and momentum transfer would again allow one to draw for each bin a Rosenbluth plot. This would, of course, be a model dependent extraction of weak response functions from the data.

It has to be investigated how sensitively the mapping $(\epsilon_{fn},\Theta_n)\mapsto(\overline{q_n},\overline{\omega_n},\Theta_n)$ depends on details of the nuclear model.

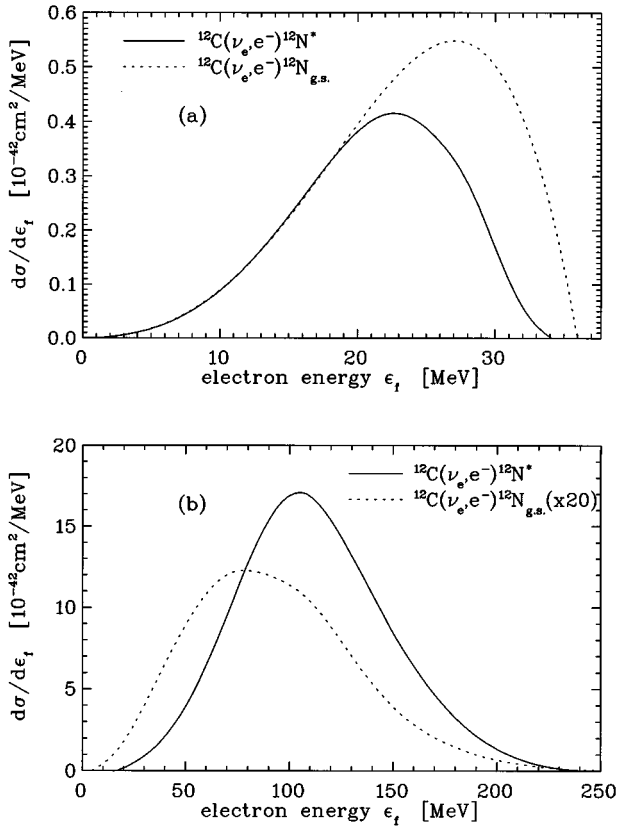

FIG. 5. Dependence of $d\sigma/d\epsilon_f$ for the $^{12}C(\nu_e,e^-)^{12}N^*$ and $^{12}C(\nu_e,e^-)^{12}N_{g.s.}$ reaction on different neutrino sources. In the upper diagram (a) the electron neutrinos have the energy distribution from muon decay, in the lower diagram (b) they are assumed to stem from $\nu_\mu \to \nu_e$ oscillations.

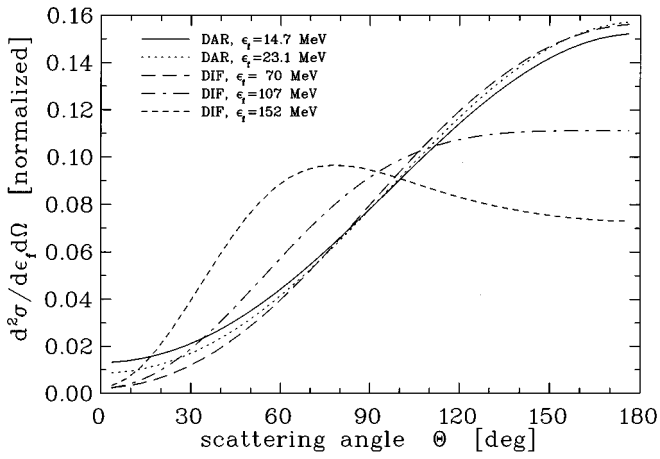

FIG. 6. Double differential cross sections for the $^{12}C(\nu_e,e^-)^{12}N^*$ reaction. The angular distribution is shown for decay-at-rest (DAR) and decay-in-flight (DIF) neutrino sources and for various final energies of the electron.

We do not present the differential cross sections plotted in Fig. 4 for the matching (ν_μ,μ^-) reactions because, as mentioned above, it is very unlikely that the angle for outgoing muons can be measured. We just state that, similar to the $^{12}C(\nu_e,e^-)^{12}N^*$ reaction, the relative Coulomb-plus-longitudinal contribution is small. Quantitatively, a reduction of σ_{CL} by 50% only lowers the total $^{12}C(\nu_\mu,\mu^-)^{12}N^*$ cross section by $\approx 8\%$. Therefore, to pin down the discrepancy between theory and experiment concerning the $^{12}C(\nu_\mu,\mu^-)X$ reaction, the important piece to check on the theoretical side is the transverse response of the nuclear model.

Note that, besides reducing the longitudinal response, also the effect of a modification of other parameters was investigated. These *parameter variations* were motivated by the hope that a possible quenching of the axial vector form factor G_A could cause a characteristic change in the shape of the differential cross sections. Unfortunately this turned out not to be the case, i.e., the shape of the differential cross sections was relatively insensitive to a reduction of G_A. From this it can be concluded that the weight of the axial current in longitudinal and transverse response functions is approximately equal. Also variations of the pseudoscalar form factor F_P, the charge and magnetic form factors of the nucleons did not leave behind significant fingerprints on the shape of the curves.

IV. NEUTRINO OSCILLATIONS AND DIFFERENTIAL CROSS SECTIONS

Thus far we have considered angle differential cross sections for neutrino scattering and now turn to cross sections differential for the energy ϵ_f of the produced lepton. As the (ν_μ,μ^-) distribution has already been published in Ref. [5], the discussion is confined to (ν_e,e^-) reactions.

In Fig. 5(a) the energy spectra of the outgoing electrons are separately shown for the transition to the ground state (dotted line) and the excited states (solid line) of ^{12}N. Here the incoming electron neutrinos have the well-known energy

distributions from pion decay at rest (DAR) and the subsequent muon decay [26]. For the exclusive reaction, since the excitation energy of the nucleus is fixed, the dotted curve is just the product of the cross section times the $n_i(\epsilon_i)$ factor describing the neutrino spectrum. For higher electron energies $n_i(\epsilon_i)$ is steeply falling and the dotted curve just reflects the decreasing ν_e spectrum. Therefore, as has been pointed out by Fetscher [27], a precise measurement of this part of the spectrum can be used to trace nonstandard couplings in muon decay. For small electron energies, on the other hand, the dotted curve is governed by the quadratic increase of the cross section according to Eq. (6).

As the solid line in Fig. 5(a) has been obtained by integrating over the contributions from the excited states in ^{12}N, it is characteristic for the excitation energies and strengths of those states. Hence a measurement of its shape would allow, at least to some extent, to check the continuum RPA model.

Let us now make the assumption that oscillations of the type $\underline{\nu_\mu} \rightarrow \underline{\nu_e}$ occur, which is quite reasonable, provided that the $\nu_\mu \rightarrow \nu_e$ candidate events seen recently by LSND [28] are real and that CP symmetry is conserved. Then these electron neutrinos would have the energy spectrum stemming from pion-in-flight decay (DIF) and Fig. 5(b) shows the corresponding $^{12}\mathrm{C}(\nu_e,e^-)^{12}\mathrm{N}_{\mathrm{g.s.}}$ (dotted) and $^{12}\mathrm{C}(\nu_e,e^-)^{12}\mathrm{N}^*$ (solid) cross sections differential for the energy of the produced electron. By comparison with Fig. 5(a), where the maximum electron energy is smaller than 36 MeV, we see that these distributions are significantly different from the standard no-oscillation signal. Therefore, provided we have good statistics, these distributions put a clear constraint on $\nu_\mu \rightarrow \nu_e$ oscillation candidate events. However, as the $^{12}\mathrm{C}(\nu_e,e^-)^{12}\mathrm{N}_{\mathrm{g.s.}}$ cross section is very small [as indicated in Fig. 5(b) it was multiplied by a factor 20 to allow comparison of its shape with that of the $^{12}\mathrm{C}(\nu_e,e^-)^{12}\mathrm{N}^*$ curve], the number of exclusive-reaction events will be too tiny for this constraint to work.

Now let us assume that enough data will be collected to plot the double differential cross section $(d^2\sigma/d\Omega d\epsilon_f)$ for the $^{12}\mathrm{C}(\nu_e,e^-)^{12}\mathrm{N}^*$ reaction. This is not unreasonable for the events induced by the neutrinos from DAR, but it is *very optimistic* for the $\nu_\mu \rightarrow \nu_e$ oscillation candidate events. However, we calculated the double differential cross sections for both neutrino sources and compare them in Fig. 6. Here the dotted and solid lines show the result for two energies of the outgoing electron, $\epsilon_f = 23.1$ MeV and $\epsilon_f = 14.7$ MeV, corresponding to the position of the maximum of the solid curve in Fig. 5(a) and to a somewhat smaller value. The dash-dotted, long-dashed, and short-dashed lines represent the angular distributions for oscillation candidate events, where the produced electron is emitted with an energy of 107 MeV, 70 MeV, and 152 MeV, respectively. We see that for high ϵ_f the differential cross sections are much less backward peaked and clearly different from the standard events induced by DAR neutrinos. So this would put another constraint on oscillation candidate events.

V. SUMMARY

In conclusion, we think that it is very promising to measure differential neutrino scattering cross sections, for the following reasons.

(1) For sufficiently accurate data it should be possible to extract the weak Coulomb longitudinal and the weak transverse response from the angular distributions. We have suggested various methods to do this. They are analogous to the Rosenbluth separation in electron scattering and should be of similar benefits. It would be the first step into an up to now unreached area: the measurement of weak nuclear response functions in neutrino scattering.

(2) For the $^{12}\mathrm{C}(\nu_e,e^-)^{12}\mathrm{N}^*$ cross section we predict a strong backward peaking of the angular distribution caused by the conserved vector current hypothesis and the calculated weights for excitation of natural and unnatural parity states in ^{12}N. A measurement would test these results.

(3) For a given neutrino spectrum the differential cross section $d\sigma/d\Omega$ determines the momentum transfer distribution $d\sigma/dq$. It is important to know this $|\vec{q}|$ dependence as well for judging the applicability of various nuclear models to the corresponding reactions as for (further) testing of nuclear models (e.g., by comparing with data for electron scattering in that range of momentum transfer).

(4) Given good statistics, (double) differential cross sections would put constraints on neutrino oscillation candidate events.

Unfortunately a quenching of the axial vector form factor G_A or modifications of the pseudoscalar form factor F_P do not leave behind significant fingerprints on the shape of the differential (ν_e,e^-) cross sections.

Finally we found that the $^{12}\mathrm{C}(\nu_\mu,\mu^-)X$ cross section is dominated by the transverse nuclear response and that the momentum transfer distribution for this reaction is broad and centered around $|\vec{q}| \approx 200$ MeV/c.

ACKNOWLEDGMENTS

I thank F.-K. Thielemann and I. Sick for helpful discussions. This work was supported by the Swiss National Science Foundation.

[1] R. C. Allen, H. H. Chen, P. J. Doe, R. Hausamann, and W. P. Lee, Phys. Rev. Lett. **64**, 1871 (1990).

[2] B. Bodmann *et al.*, KARMEN Collaboration, Phys. Lett. B **267**, 321 (1991).

[3] B. Bodmann *et al.*, KARMEN Collaboration, Phys. Lett. B **280**, 198 (1992).

[4] W. C. Louis, LAMFP Research Report No. LA-UR-89-3764, 1989.

[5] E. Kolbe, K. Langanke, F.-K. Thielemann, and P. Vogel, Phys. Rev. C **52**, 3437 (1995), and references therein.

[6] T. S. Kosmas and E. Oset, Phys. Rev. C **53**, 1409 (1996).

[7] M. Albert *et al.*, Phys. Rev. C **51**, 1065 (1995).

[8] M. Buballa, S. Drożdż, S. Krewald, and J. Speth, Ann. Phys. **208**, 346 (1991).
[9] E. Kolbe, K. Langanke, S. Krewald, and F.-K. Thielemann, Nucl. Phys. **A540**, 599 (1992).
[10] J. D. Walecka, in *Muon Physics*, edited by V. W. Hughes and C. S. Wu (Academic Press, New York, 1975), p. 113.
[11] K. Nakayama, S. Drożdż, S. Krewald, and J. Speth, Nucl. Phys. **A470**, 573 (1987).
[12] R. Machleidt, K. Holinde, and Ch. Elster, Phys. Rep. **149**, 1 (1987).
[13] S. Krewald, K. Nakayama, and J. Speth, Phys. Rep. **161**, 103 (1988).
[14] E. Kolbe, K. Langanke, and P. Vogel, Phys. Rev. C **50**, 2576 (1994).
[15] S. Boffi, C. Giusti, and F. D. Pacati, Phys. Rep. **226**, 1 (1993).
[16] E. Kolbe, K. Langanke, and S. Krewald, Phys. Rev. C **49**, 1122 (1994).
[17] S. L. Mintz and M. Pourkaviani, Nucl. Phys. **A594**, 346 (1995); the authors estimate their error in the 25–30 % range.
[18] H. J. Kim, preliminary results from the LSND Collaboration presented at the 1996 PANIC conference.
[19] T. W. Donnelly, Phys. Lett. **43B**, 93 (1973).
[20] G. Drexlin, KARMEN Collaboration, data presented on the Nuclear Physics Spring Meeting of the DPG, Cologne, 1995.
[21] This number is the difference between the (inclusive) $^{12}\mathrm{C}(\nu_e,e^-)X$ cross section given in M. Pourkaviani and S. L. Mintz, Nucl. Phys. **A573**, 501 (1994), and the (exclusive) contribution to the $^{12}\mathrm{N}_{\mathrm{g.s.}}$ given in Ref. [23].
[22] M. Fukugita, Y. Kohyama, and K. Kubodera, Phys. Lett. B **212**, 139 (1988).
[23] S. L. Mintz and M. Pourkaviani, Phys. Rev. C **40**, 2458 (1989). Note that, due to different flux normalization, the cross section given in this paper must be renormalized for comparison with the experiments.
[24] S. L. Adler, Phys. Rev. **135**, B963 (1964).
[25] J. Jourdan, Nucl. Phys. **A603**, 117 (1996), and references therein.
[26] H. Überall, Nuovo Cimento **23**, 219 (1962).
[27] W. Fetscher, Phys. Rev. Lett. **69**, 2758 (1992); **71**, 2522(E) (1993); C. Greub, D. Wyler, and W. Fetscher, Phys. Lett. B **324**, 109 (1994); **329**, 526(E) (1994).
[28] C. Athanassopoulos *et al.*, Phys. Rev. Lett. **75**, 2650 (1995).